Article

Cell Host & Microbe

Ultrapotent miniproteins targeting the SARS-CoV-2 receptor-binding domain protect against infection and disease

Graphical abstract

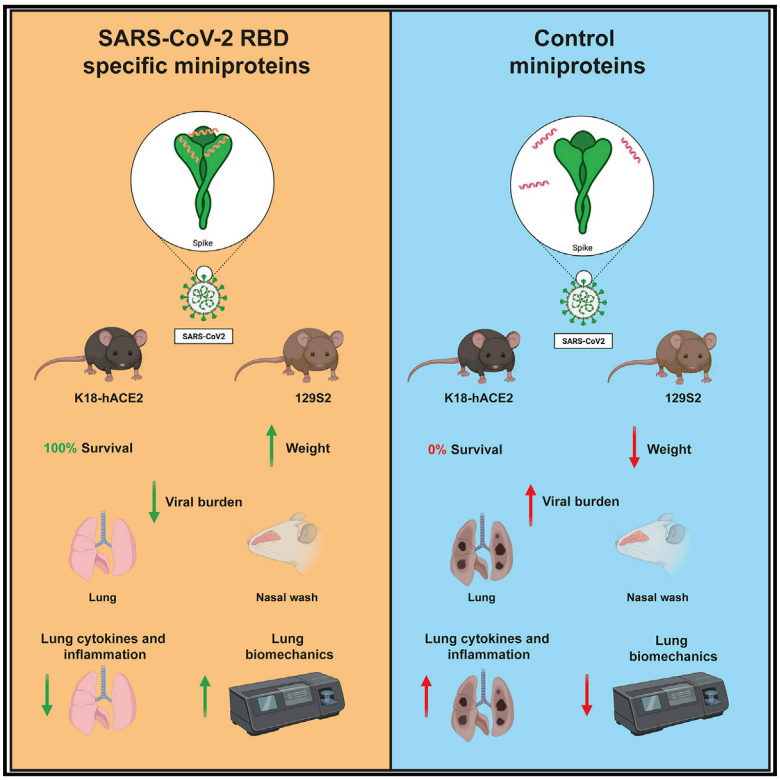

Highlights

- SARS-CoV-2 RBD-specific miniproteins confer 100% survival against lethal challenge
- Miniproteins prevent SARS-CoV-2-induced lung inflammation and pathology
- One miniprotein dose protects when given between D-5 and D+3 relative to infection
- Miniproteins inhibit historical, circulating, and emerging SARS-CoV-2 strains

Authors

James Brett Case, Rita E. Chen, Longxing Cao, ..., Lance Stewart, David Baker, Michael S. Diamond

Correspondence

diamond@wusm.wustl.edu

In brief

Case et al. show that *de novo*-designed SARS-CoV-2 RBD-specific miniproteins administered as prophylaxis or therapy protect mice against SARS-CoV-2-mediated disease, inflammation, and pathology. Injected or intranasal administration of miniproteins showed efficacy when given any time over an 8-day treatment window.

Case et al., 2021, Cell Host & Microbe *29*, 1–11
July 14, 2021
https://doi.org/10.1016/j.chom.2021.06.008

CellPress

Cell Host & Microbe

CellPress

Article

Ultrapotent miniproteins targeting the SARS-CoV-2 receptor-binding domain protect against infection and disease

James Brett Case,[1] Rita E. Chen,[1,2] Longxing Cao,[3,4] Baoling Ying,[1] Emma S. Winkler,[1,2] Max Johnson,[3,4] Inna Goreshnik,[3,4] Minh N. Pham,[3,4] Swathi Shrihari,[1] Natasha M. Kafai,[1,2] Adam L. Bailey,[2] Xuping Xie,[5] Pei-Yong Shi,[5,6,7] Rashmi Ravichandran,[3,4] Lauren Carter,[3,4] Lance Stewart,[3,4] David Baker,[3,4,8] and Michael S. Diamond[1,2,9,10,11,*]

[1]Department of Medicine, Washington University School of Medicine, St. Louis, MO 63110, USA
[2]Department of Pathology & Immunology, Washington University School of Medicine, St. Louis, MO 63110, USA
[3]Department of Biochemistry, University of Washington, Seattle, WA 98195, USA
[4]Institute for Protein Design, University of Washington, Seattle, WA 98195, USA
[5]Department of Biochemistry and Molecular Biology, University of Texas Medical Branch, Galveston, TX 77555, USA
[6]Institute for Human Infections and Immunity, University of Texas Medical Branch, Galveston, TX 77555, USA
[7]Sealy Institute for Vaccine Sciences, University of Texas Medical Branch, Galveston, TX 77555, USA
[8]Howard Hughes Medical Institute, University of Washington, Seattle, WA 98195, USA
[9]Department of Molecular Microbiology, Washington University School of Medicine, St. Louis, MO 63110, USA
[10]The Andrew M. and Jane M. Bursky Center for Human Immunology and Immunotherapy Programs, Washington University School of Medicine, St. Louis, MO 63110, USA
[11]Lead contact
*Correspondence: diamond@wusm.wustl.edu
https://doi.org/10.1016/j.chom.2021.06.008

SUMMARY

Despite the introduction of public health measures and spike protein-based vaccines to mitigate the COVID-19 pandemic, SARS-CoV-2 infections and deaths continue to have a global impact. Previously, we used a structural design approach to develop picomolar range miniproteins targeting the SARS-CoV-2 spike receptor-binding domain. Here, we investigated the capacity of modified versions of one lead miniprotein, LCB1, to protect against SARS-CoV-2-mediated lung disease in mice. Systemic administration of LCB1-Fc reduced viral burden, diminished immune cell infiltration and inflammation, and completely prevented lung disease and pathology. A single intranasal dose of LCB1v1.3 reduced SARS-CoV-2 infection in the lung when given as many as 5 days before or 2 days after virus inoculation. Importantly, LCB1v1.3 protected *in vivo* against a historical strain (WA1/2020), an emerging B.1.1.7 strain, and a strain encoding key E484K and N501Y spike protein substitutions. These data support development of LCB1v1.3 for prevention or treatment of SARS-CoV-2 infection.

INTRODUCTION

Severe acute respiratory syndrome coronavirus 2 (SARS-CoV-2), the cause of the coronavirus disease 2019 (COVID-19) pandemic, has resulted in global disease, suffering, and economic hardship. Despite implementation of public health measures, SARS-CoV-2 transmission persists principally through human-to-human spread (Day, 2020; Li et al., 2020; Petersen et al., 2020). SARS-CoV-2-induced clinical manifestations range from asymptomatic infection to severe pneumonia, multi-organ failure, and death. Although the underlying mechanisms that dictate disease severity are poorly understood, the immunocompromised, the elderly, and those with specific comorbidities (e.g., history of cardiovascular disease, diabetes, or obesity) are at increased risk for poor outcome (Zhou et al., 2020).

SARS-CoV-2 entry into target cells is facilitated by the spike glycoprotein through binding to its principal receptor, angiotensin converting enzyme 2 (ACE2) (Hoffmann et al., 2020; Letko et al., 2020). Once the virus is attached to the cell surface, the spike protein is cleaved by the cell membrane-associated protease, TMPRSS2, resulting in membrane fusion and release of the viral RNA genome into the host cell cytoplasm (Hoffmann et al., 2020; Matsuyama et al., 2020). As the dominant antigen on the surface of the virion, the spike protein is the primary target of antibody-based countermeasures (Jeyanathan et al., 2020; Krammer, 2020). At present, a small number of antibody therapies and vaccines have been granted emergency use authorization (EUA) by the United States Food and Drug Administration to prevent or treat SARS-CoV-2 infection and disease. Nonetheless, viral evolution and the emergence of SARS-CoV-2 variants in the United Kingdom (B.1.1.7 [alpha]), South Africa (B.1.351 [beta]), Brazil (B.1.1.28 [gamma]), India (B.1.617.2 [delta]), and elsewhere jeopardize these countermeasures through potential loss of binding and diminished neutralization

Please cite this article in press as: Case et al., Ultrapotent miniproteins targeting the SARS-CoV-2 receptor-binding domain protect against infection and disease, Cell Host & Microbe (2021), https://doi.org/10.1016/j.chom.2021.06.008

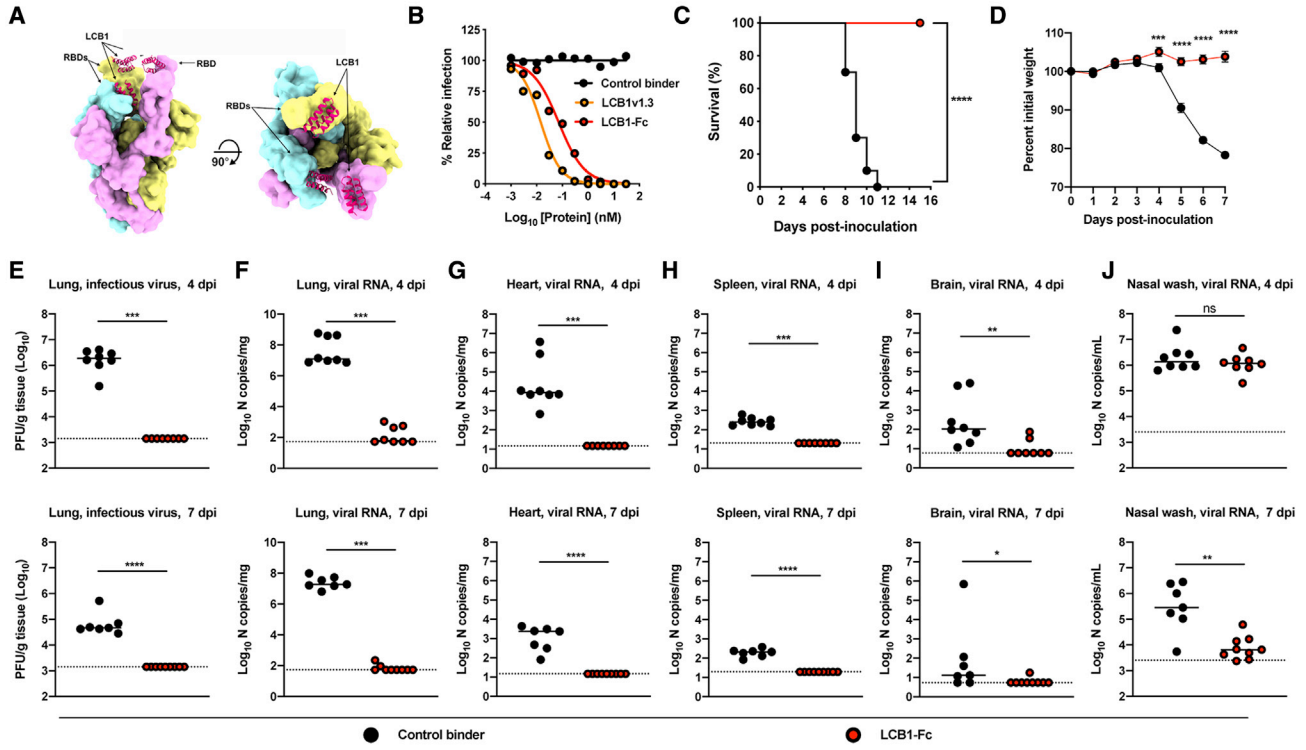

Figure 1. LCB1-Fc prophylaxis protects against SARS-CoV-2 infection

(A) Molecular surface representation of three LCB1v1.3 miniproteins bound to individual protomers of the SARS-CoV-2 spike protein trimer (left: side view; right: top view).

(B) Neutralization curves of LCB1v1.3, LCB1-Fc or control binder against a SARS-CoV-2 WA1/2020 isolate (EC_{50} values: 14.4 pM, 71.8 pM, and >10,000 nM, respectively; average of two experiments, each performed in duplicate).

(C) 8-week-old female K18-hACE2 mice received 250 μg of LCB1-Fc or control binder by i.p. injection 1 day prior to i.n. inoculation with a lethal dose (10^3 PFU/mouse) of SARS-CoV-2. Animals were monitored daily for survival (n = 10 per group); two independent experiments: Mantel-Cox log-rank test; ****$p < 0.0001$.

(D–J) 7- to 8-week-old female and male K18-hACE2 mice received 250 μg of LCB1-Fc or control binder by i.p. injection 1 day prior to i.n. inoculation with 10^3 PFU of SARS-CoV-2. Tissues were collected at 4 and 7 dpi. (D) Weight change following LCB1-Fc administration (mean ± SEM; n = 8, two experiments: two-way ANOVA with Sidak's post-test: ***$p < 0.001$, ****$p < 0.0001$). (E) Infectious virus measured by plaque assay at 4 or 7 dpi in the lung (n = 8, two experiments: Mann-Whitney test; ***$p < 0.001$). (F–J) Viral RNA levels at 4 or 7 dpi in the lung, heart, spleen, brain, or nasal wash (n = 8, two experiments: Mann-Whitney test: ns, not significant, *$p < 0.05$, **$p < 0.01$, ***$p < 0.001$, ****$p < 0.0001$).

See also Figure S1 and S2.

(Galloway et al., 2021; Leung et al., 2021; Tegally et al., 2020; Voloch et al., 2021).

We recently generated a panel of short, 56-amino-acid miniproteins that bind the SARS-CoV-2 receptor-binding domain (RBD) of spike with high affinity and potently neutralize authentic virus in cell culture with half-maximal effective concentration (EC_{50}) values < 30 pM (Cao et al., 2020). Here, we evaluated the *in vivo* efficacy of one of these miniprotein binders, LCB1, against SARS-CoV-2 and its variants of concern in two immunocompetent mouse models, human ACE2 (hACE2)-expressing transgenic mice (Golden et al., 2020; Winkler et al., 2020) and non-hACE2 transgenic 129S2 mice (Gu et al., 2020; Rathnasinghe et al., 2021). For our *in vivo* experiments, we evaluated two versions of LCB1: (1) an Fc-modified bivalent form, LCB1-hIgG-Fc9 (LCB1-Fc), which should extend half-life *in vivo* and engage effector arms of the immune system; and (2) a further optimized, monomeric form of LCB1 lacking an Fc domain, LCB1v1.3. Intraperitoneal administration of LCB1-Fc at 1 day pre- or up to 3 days post-SARS-CoV-2 exposure conferred substantial protection including an absence of weight loss, reductions in viral burden approaching the limit of detection, and inhibition of lung inflammation, pathology, and death. Intranasal (i.n.) delivery of LCB1v1.3 conferred protection as many as 5 days before or 2 days after SARS-CoV-2 inoculation. Dosing experiments revealed that LCB1v1.3 retained efficacy at pharmacologically attainable concentrations and was weakly immunogenic. Most importantly, LCB1v1.3 protected animals against the currently emerging B.1.1.7 variant and a SARS-CoV-2 strain encoding key spike substitutions, E484K and N501Y, present in both B.1.351 and B.1.1.28 variants of concern. Overall, these studies establish LCB1-Fc and LCB1v1.3 as possible treatments to prevent or mitigate COVID-19 disease.

RESULTS

LCB1-Fc prophylaxis limits viral burden and clinical disease

Using computational design and functional screens, we previously designed LCB1 as a potent miniprotein inhibitor of SARS-CoV-2 infection, which acts by directly binding to individual RBDs of the viral spike trimer (Figure 1A) (Cao et al., 2020).

Please cite this article in press as: Case et al., Ultrapotent miniproteins targeting the SARS-CoV-2 receptor-binding domain protect against infection and disease, Cell Host & Microbe (2021), https://doi.org/10.1016/j.chom.2021.06.008

CellPress

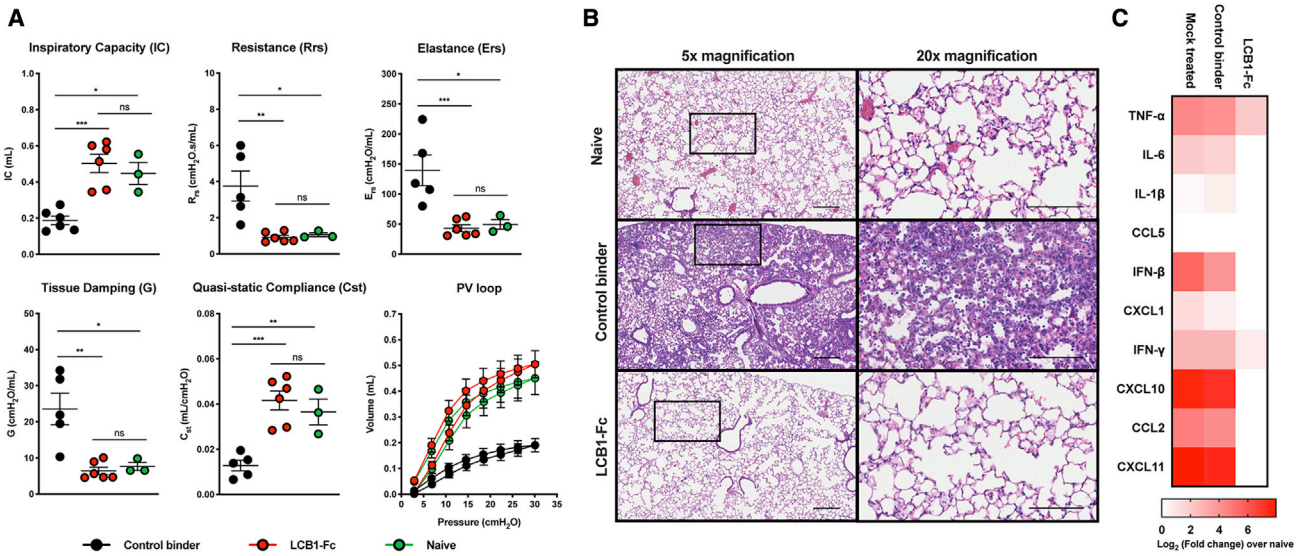

Figure 2. LCB1-Fc prophylaxis prevents SARS-CoV-2-mediated lung disease

(A) 7- to 8-week-old female and male K18-hACE2 mice received 250 μg of LCB1-Fc or control binder by i.p. injection 1 day prior to i.n. inoculation with 10^3 PFU of SARS-CoV-2. Respiratory mechanics parameters: inspiratory capacity, resistance, elastance tissue damping, quasi-static compliance, and pressure-volume loops measured at 7 dpi (mean ± SEM, n = 3–6, two experiments: two-way ANOVA with Tukey's post-test: ns, not significant, *p < 0.05, **p < 0.01, ***p < 0.001 between indicated groups).

(B) Hematoxylin and eosin staining of lung sections from mice treated at D−1 and collected at 7 dpi with SARS-CoV-2. Images show low (left) and high (right; boxed region from left) magnification. Scale bars for all images, 100 μm. Representative images from n = 3 mice per group.

(C) Heat map of cytokine mRNA levels from lung tissues of SARS-CoV-2-infected mice at 4 dpi. For each cytokine, the fold change was calculated relative to age-matched naive control animals after normalization to *Gapdh* and the Log_2(fold change) was plotted (n = 6–8 mice/group relative to n = 3 naive controls).

See also Figure S3.

We modified LCB1 to generate two versions for *in vivo* testing: (1) we introduced polar mutations into LCB1 to increase expression yield and solubility without altering RBD binding (LCB1v1.3) and (2) we modified LCB1 by fusing it to a human IgG1 Fc domain (LCB1-Fc) to enhance bioavailability. LCB1v1.3 and LCB1-Fc bound avidly to a single RBD within the spike trimer with dissociation constants (K_D) of less than 625 and 156 pM, respectively (Figure S1). LCB1v1.3 and LCB1-Fc also potently neutralized an authentic SARS-CoV-2 isolate (2019n-CoV/USA_WA1/2020 [WA1/2020]) (EC_{50} of 14.4 and 71.8 pM, respectively; Figure 1B).

To determine the protective potential of these miniproteins against SARS-CoV-2, we utilized K18 human hACE2-expressing transgenic mice, which develop severe lung infection and disease after i.n. inoculation of SARS-CoV-2 (Golden et al., 2020; Winkler et al., 2020). In prophylaxis studies, a single 250-μg (~10 mg/kg) dose of LCB1-Fc administered by intraperitoneal (i.p.) injection 1 day prior to i.n. inoculation with a lethal dose (10^3 plaque-forming units [PFU]) of SARS-CoV-2 WA1/2020 prevented weight loss and death compared to animals given a control protein (influenza A virus hemagglutinin minibinder; Chevalier et al., 2017) designed using similar computational methods (Figures 1C and 1D). After LCB1-Fc prophylaxis, infectious virus was not detected in the lungs at 4 or 7 days post-infection (dpi), whereas high levels were observed in animals administered control protein (Figure 1E, top and bottom). Similarly, viral RNA levels in the lung, heart, spleen, and brain of LCB1-Fc-treated animals were at or near the limit of detection of the assay at 4 or 7 dpi (Figures 1F–1I). LCB1-Fc treatment had no effect on viral RNA levels in nasal wash samples obtained at 4 dpi (Figure 1J), results that are similar to a recent study of a neutralizing human antibody in hamsters (Zhou et al., 2021). However, viral RNA levels were reduced at 7 dpi, suggesting that LCB1-Fc treatment accelerated viral clearance or prevented spread in the upper respiratory tract.

To corroborate our findings, we tested the efficacy of LCB1-Fc in a non-transgenic 129S2 mouse model of SARS-CoV-2 infection with two strains containing the mouse-adapting N501Y substitution (Gu et al., 2020; Rathnasinghe et al., 2021): a recombinant WA1/2020 strain containing N501Y and D614G substitutions and a B.1.1.7 natural isolate. Prophylaxis with 250 μg of LCB1-Fc, but not control binder, at D-1 reduced viral burden in the lungs and nasal washes of 129S2 mice infected with either SARS-CoV-2 strain (Figure S2).

Diffuse alveolar damage, inflammation, and pneumonia are manifestations of COVID-19 lung disease, culminating in respiratory failure and a requirement for mechanical ventilation (Johnson et al., 2020; Kordzadeh-Kermani et al., 2020). We evaluated the capacity of LCB1-Fc to prevent the compromised lung function observed after SARS-CoV-2 infection of K18-hACE2 mice (Winkler et al., 2020). At 7 dpi, mechanical ventilation tests of lung biomechanics in animals treated with LCB1-Fc showed no difference from naive animals (Figure 2A), whereas mice receiving the control binder protein showed decreased inspiratory capacity and lung compliance as well as increased pulmonary resistance, elastance, and tissue damping, all consistent with compromised lung function. These biophysical properties resulted in disparate pressure-volume loops between control binder and LCB1-Fc-treated or naive animals. We also assessed

Please cite this article in press as: Case et al., Ultrapotent miniproteins targeting the SARS-CoV-2 receptor-binding domain protect against infection and disease, Cell Host & Microbe (2021), https://doi.org/10.1016/j.chom.2021.06.008

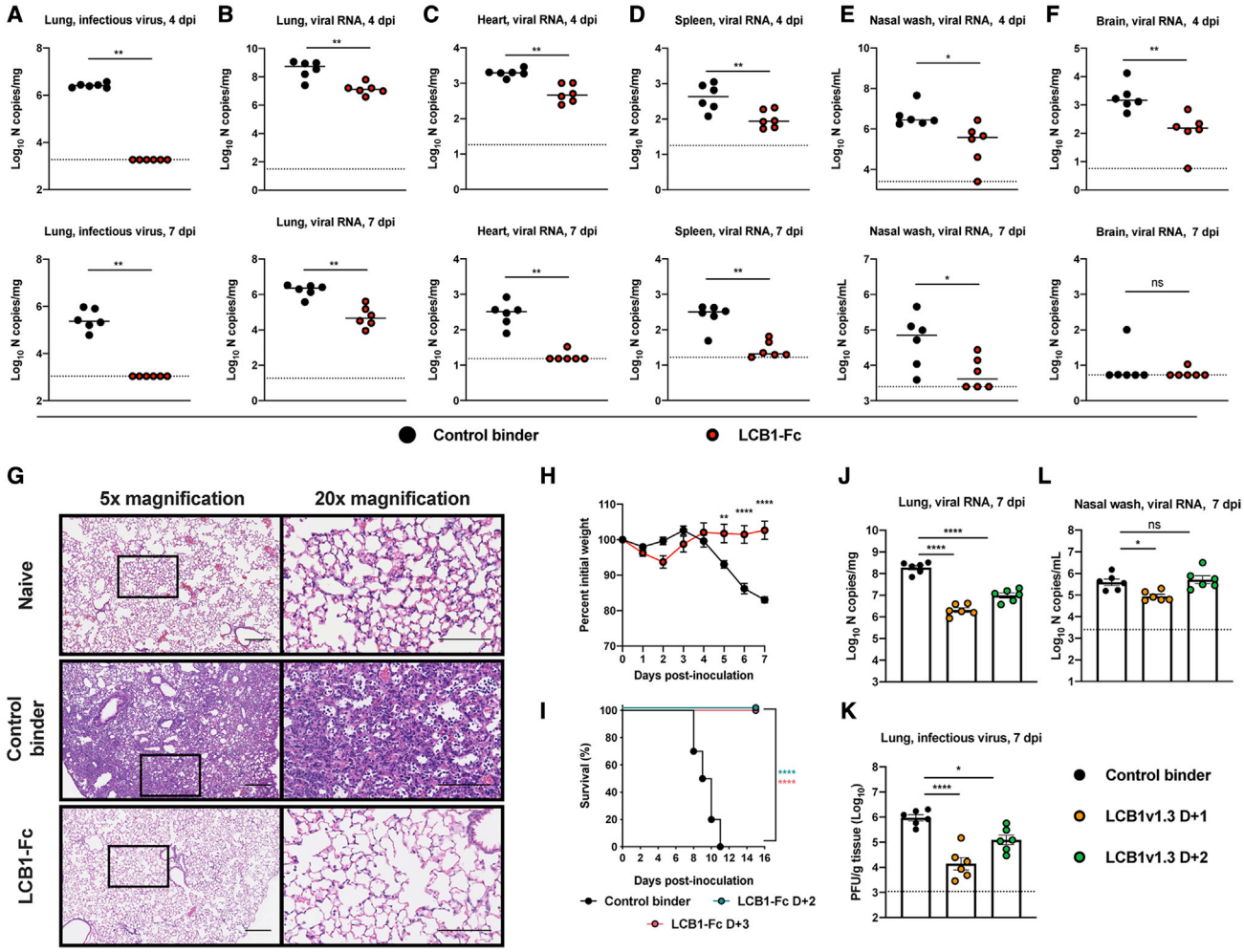

Figure 3. Post-exposure delivery of anti-RBD binders reduces SARS-CoV-2 burden

(A–G) 7- to 8-week-old female and male K18-hACE2 mice received 250 μg of LCB1-Fc or control binder by i.p. injection 1 day after i.n. inoculation with 10^3 PFU of SARS-CoV-2. Tissues were collected at 4 or 7 dpi. (A) Infectious virus in the lung measured by plaque assay at 4 or 7 dpi in the lung (n = 6, two experiments: $^{**}p < 0.01$). (B–F) Viral RNA levels at 4 or 7 dpi in the lung, heart, spleen, nasal wash, or brain (n = 6, two experiments: Mann-Whitney test: ns, not significant, $^{*}p < 0.05$, $^{**}p < 0.01$). (G) Hematoxylin and eosin staining of lung sections from mice treated at D+1 and collected at 7 dpi with SARS-CoV-2. Images show low (left) and high (right; boxed region from left) magnification. Scale bars for all images, 100 μm. Representative images from n = 3 mice per group.

(H) Weight change following LCB1-Fc administration (mean ± SEM; n = 6, two experiments: two-way ANOVA with Sidak's post-test: $^{**}p < 0.01$, $^{****}p < 0.0001$).

(I) 8-week-old female K18-hACE2 mice were inoculated with a lethal dose (10^3 PFU) of SARS-CoV-2 by i.n. administration. At D+2 or D+3, they received a single 250-μg dose of LCB1-Fc or control binder by i.p. injection. Animals were monitored daily for survival (n = 10 per group, two experiments: Mantel-Cox log-rank test; $^{****}p < 0.0001$).

(J–L) 7- to 8-week-old male K18-hACE2 mice received a single 50-μg i.n. dose of LCB1v1.3 or control binder at 1 or 2 days post-inoculation with 10^3 PFU of SARS-CoV-2. Viral RNA levels at 7 dpi in the lung (J), nasal wash (L), or infectious virus in the lung (K) were determined (mean ± SEM, n = 6, two experiments: one-way ANOVA: ns, not significant, $^{*}p < 0.05$, $^{****}p < 0.0001$).

See also Figure S4.

the effect of LCB1-Fc treatment on SARS-CoV-2-induced lung pathology. Lung sections of animals collected at 7 dpi with SARS-CoV-2 showed widespread inflammation characterized by a cellular infiltrate and airspace consolidation in control protein-treated, but not LCB1-Fc treated or naive mice (Figure 2B). At 4 dpi, inflammatory cytokine and chemokine RNA signatures in the lung were absent in LCB1-Fc-treated but not control binder or mock-treated animals, suggesting that LCB1-Fc treatment prevents virus infection and inflammation in the lung (Figures 2C and S3).

Post-exposure therapy with anti-RBD binders reduces viral burden

To evaluate its efficacy in a post-exposure setting, we administered 250 μg of LCB1-Fc by i.p. injection at 1 dpi. Therapy with LCB1-Fc reduced viral burden in all tested tissues at 4 and 7 dpi (Figures 3A–3F), and infectious virus was not recovered from the lungs of LCB1-Fc-treated animals collected at either time point. Lung sections confirmed that therapy with LCB1-Fc improved pathological outcome (Figure 3G). At 7 dpi, immune cell infiltrates were absent in the lung sections of LCB1-Fc-

Please cite this article in press as: Case et al., Ultrapotent miniproteins targeting the SARS-CoV-2 receptor-binding domain protect against infection and disease, Cell Host & Microbe (2021), https://doi.org/10.1016/j.chom.2021.06.008

treated but not control binder-treated animals. Weight loss was absent in LCB1-Fc but not control binder-treated animals (Figure 3H). To evaluate further the therapeutic window of LCB1-Fc, we inoculated K18-hACE2 mice with a lethal (10^3 PFU) dose of SARS-CoV-2 and treated animals with a single 250 μg of control binder or LCB1-Fc beginning at 2 (D+2) or 3 (D+3) days after infection. Whereas control binder-treated animals succumbed to infection by day 11 post-inoculation, all LCB1-Fc-treated mice survived (Figure 3I). These data confirm the therapeutic potential of LCB1-Fc.

We next tested the efficacy of LCB1v1.3 as an i.n.-delivered post-exposure therapy. I.n. delivery might enable self-administration of an anti-SARS-CoV-2 biological drug. Indeed, miniprotein inhibitors against influenza virus have shown efficacy by nasal delivery (Chevalier et al., 2017). For these studies, we used LCB1v1.3 because of its small 9.1-kilodalton size (versus an Fc fusion protein), which allows for binding to an increased number of RBD molecules for a given mass dose and greater neutralizing activity (Figure 1B). Whereas high levels of SARS-CoV-2 RNA and infectious virus were detected in the lungs and other peripheral tissues of control binder-treated animals at 7 dpi, infection was reduced in animals receiving 50 μg of LCB1v1.3 by i.n. administration at D+1 or D+2 after inoculation with SARS-CoV-2 (Figures 3J, 3K, and S4). Levels of viral RNA were reduced in the nasal washes of animals receiving LCB1v1.3 after treatment at D+1 but not D+2 compared to control binder-treated animals (Figure 3L).

Intranasal delivery of LCB1v1.3 confers protection against SARS-CoV-2 when administered up to 5 days before infection

We next evaluated the durability of LCB1v1.3 administered via i.n. prophylaxis. At 5 days, 3 days, 1 day, or 6 h prior to inoculation with 10^3 PFU of SARS-CoV-2, K18-hACE2 transgenic mice received a single 50-μg i.n. dose of LCB1v1.3 or the control binder. At 4 or 7 dpi, viral burden in tissues was determined by RT-qPCR. As expected, protection by LCB1v1.3 was better when administered closer to the time of SARS-CoV-2 exposure, as reflected by greater reductions in viral load and weight loss (Figures 4A–4D and S5). However, even mice receiving LCB1v1.3 5 days prior to inoculation and collected at 7 dpi showed an approximately 400-fold reduction viral RNA levels in the lung compared to control binder-treated animals. Regardless of the collection time point, lung viral RNA levels were reduced in animals receiving LCB1v1.3 3 days prior to inoculation with SARS-CoV-2.

An important consideration for our binders as a potential therapy is scalable production and feasible dosing. To begin to address this issue, we tested a range of i.n. doses of LCB1v1.3 for efficacy when given 1 day prior to SARS-CoV-2 inoculation (Figures 4E–4J). Treatment with as little as 2 μg (0.1 mg/kg) of LCB1v1.3 prevented SARS-CoV-2-induced weight loss. Doses of 10 μg (0.5 mg/kg) or greater of LCB1v1.3 reduced viral RNA levels in the lung, heart, and spleen at 7 dpi relative to control binder-treated animals. Moreover, animals receiving a 50-μg dose of LCB1v1.3 showed minimal, if any, lung inflammation (Figure 4K). Collectively, these results indicate that even low doses of LCB1v1.3, when administered via an i.n. route prior to exposure, can limit SARS-CoV-2 infection and disease in the stringent K18-hACE transgenic mouse model of pathogenesis.

LCB1v1.3 is weakly immunogenic and displays desirable pharmacokinetic properties

One concern for biological drugs is their potential immunogenicity, which could limit bioavailability and efficacy. To begin to address this concern, we treated K18-hACE2 transgenic mice with 50 μg of control binder or LCB1v1.3 every 3 days for a total of 18 days (Figure 5A). At this time, we collected sera and assessed the presence of anti-LCB1v1.3 antibodies. Only one of ten mice developed IgG antibodies against LCB1v1.3 (Figure 5B). To determine if repeated dosing affected LCB1v1.3-mediated protection, we challenged the cohort with 10^3 PFU of SARS-CoV-2. Again, substantial protection against weight loss (Figure 5C) and viral infection in the lung and other organs was observed in all animals receiving LCB1v1.3 (Figures 5D–5H).

Based on the relative reductions in lung viral RNA levels seen in our time-of-prophylaxis experiments (Figures 4A–4D) and dose reduction experiments (Figures 4E–4J), we speculated that the half-life of i.n. administered LCB1v1.3 is approximately 12–24 h. To gain insight into the pharmacokinetics of LCB1v1.3 and LCB1-Fc in mice, we used a functional neutralization assay to assess the inhibitory activity in different specimens against WA1/2020 SARS-CoV-2. C57BL/6J mice were treated with 200 μg of LCB1v1.3 by i.n. administration or 250 μg LCB1-Fc by i.p. injection (Figures 5I and 5K). For LCB1v1.3 and LCB1-Fc-treated mice, serum and tissues were collected at 1, 8, 24, and 48 h or 24, 48, and 72 h post-treatment, respectively (Figures 5J and 5L). For LCB1v1.3 in the serum or nasal washes, the mean EC_{50} value per mL decreased to the limit of detection by 48 h. Nonetheless, at 48 h, substantial levels of neutralizing activity remained present within the lungs and nasal turbinates, with approximately 10-fold reductions seen at 24-h intervals. LCB1-Fc levels in the sera remained constant for each day tested, and neutralizing activity was present in the lungs on day 3 post-administration. In addition, we performed quantitative ELISAs using the same specimens (Figure 5M), which yielded results consistent with our neutralization activity time-course measurements. Together, these data suggest that the pharmacodynamic and pharmacokinetic half-lives of LCB1v1.3 and LCB1-Fc at key sites of viral replication are sufficient to provide protection for several days after a single dose.

LCB1v1.3 protects against emerging SARS-CoV-2 variants

The emergence of variant strains harboring possible escape mutations is of great concern for antibody-based countermeasures that were designed against historical SARS-CoV-2 spike proteins (Chen et al., 2021; Wang et al., 2021a, 2021b; Wibmer et al., 2021). Accordingly, we evaluated the activity of LCB1v1.3 against a B.1.1.7 isolate containing deletions at 69–70 and 144–145 and substitutions at N501Y, A570D, D614G, and P681H, and against a recombinant WA1/2020 strain containing key substitutions present in the B.1.351 and B.1.1.28 variant strains at residues E484K, N501Y, and D614G (Xie et al., 2021). Although the neutralizing activity of LCB1v1.3 against the B.1.1.7 and WA1/2020-E484K/N501Y/D614G strains was approximately 45- to 50-fold lower than for the WA1/2020

Please cite this article in press as: Case et al., Ultrapotent miniproteins targeting the SARS-CoV-2 receptor-binding domain protect against infection and disease, Cell Host & Microbe (2021), https://doi.org/10.1016/j.chom.2021.06.008

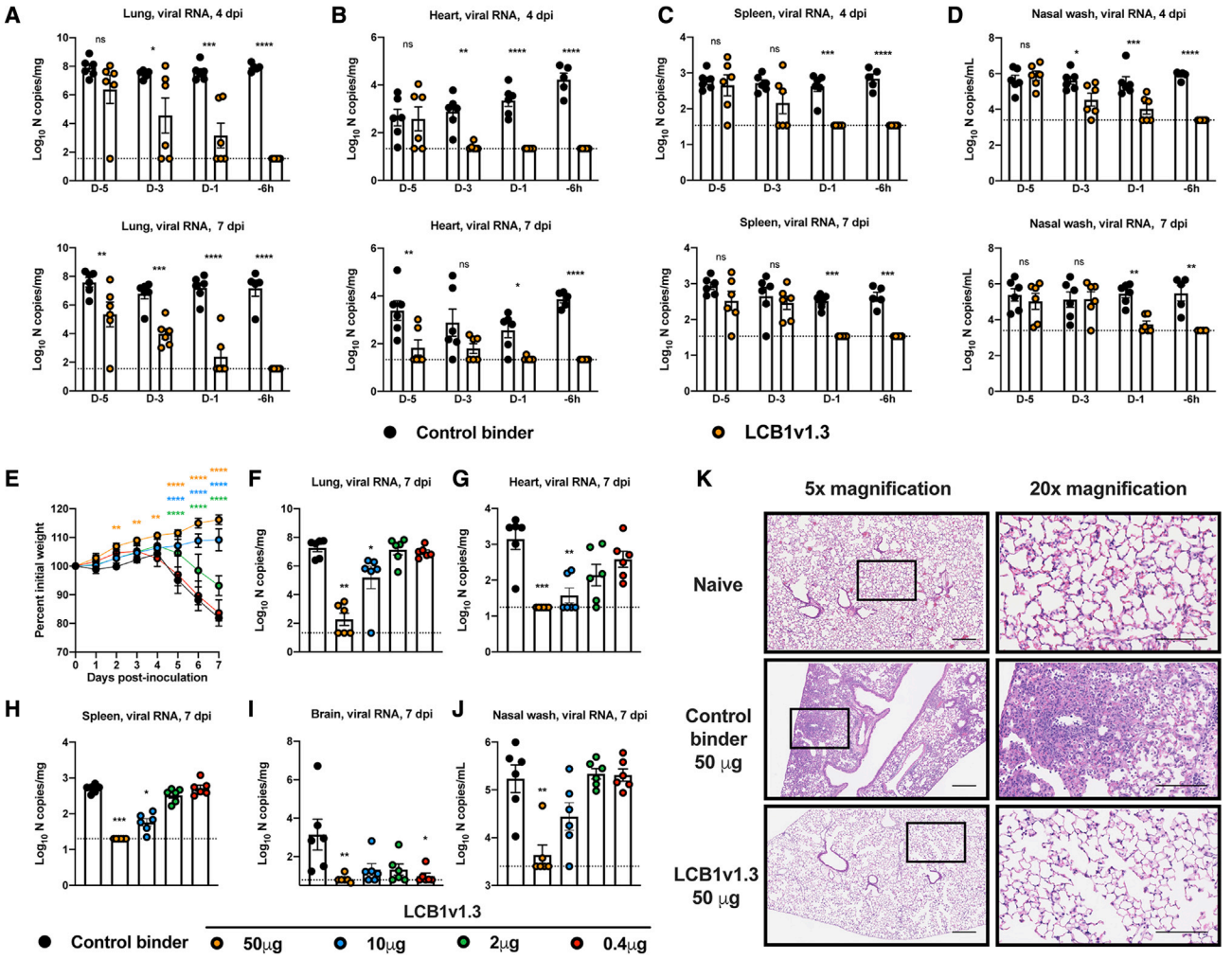

Figure 4. Intranasal administration of LCB1v1.3 reduces viral infection even when given 5 days prior to SARS-CoV-2 exposure

(A–D) 7- to 8-week-old female K18-hACE2 mice received a single i.n. 50-μg dose of LCB1v1.3 or control binder at the indicated time prior to i.n. inoculation with 10^3 PFU of SARS-CoV-2. Tissues were collected at 4 or 7 dpi and viral RNA levels were determined (mean ± SEM, n = 5–6 animals per group, two-experiments: two-way ANOVA with Sidak's post-test: ns, not significant, *p < 0.05, **p < 0.01, ***p < 0.001, ****p < 0.0001).

(E–J) 7- to 8-week-old female K18-hACE2 transgenic mice received the indicated i.n. dose of LCB1v1.3 or control binder at 1 day prior to i.n. inoculation with 10^3 PFU of SARS-CoV-2. (E) Weight change following LCB1v1.3 or control binder administration (mean ± SEM; n = 6, two experiments: two-way ANOVA with Sidak's post-test compared to the control binder treated group: **p < 0.01, ****p < 0.0001). (F–J) Viral RNA levels at 7 dpi in the lung, heart, spleen, brain, or nasal wash (mean ± SEM, n = 6, two experiments: Kruskal-Wallis ANOVA with Dunn's post-test: *p < 0.05, **p < 0.01, ***p < 0.001).

(K) Hematoxylin and eosin staining of lung sections from mice treated with a single i.n. 50-μg dose of LCB1v1.3 or control binder at D−1 and collected at 7 dpi with SARS-CoV-2. Images show low (left) and high (right; boxed region from left) magnification.

Scale bars for all images, 100 μm. Representative images from n = 3 mice per group. See also Figure S5.

strain, the EC_{50} values still were ~800 pM and 667 pM, respectively (Figure S6). To determine whether LCB1v1.3 could protect *in vivo* against SARS-CoV-2 strains with spike protein substitutions found in variants of concern, we treated K18-hACE2 transgenic mice with a single i.n. 50-μg dose of LCB1v1.3 or control binder 1 day prior to inoculation with 10^3 PFU of B.1.1.7 or a recombinant WA1/2020 strain with E484K/N501/D614G mutations. Notably, LCB1v1.3 treatment before challenge with either variant strain protected against weight loss (Figures 6A and 6G) and viral infection in all tissues collected at 6 dpi (Figures 6B–6F and 6H–6L). We also tested the durability of LCB1v1.3 prophylaxis against the WA1/2020-E484K/N501Y/D614G strain when administered by i.n. route. Animals receiving LCB1v1.3 at D-5 or D-3 prior to inoculation with WA1/2020-E484K/N501Y/D614G gained weight (Figure 6M) and had reduced viral RNA levels in the lungs (Figure 6N) compared to control binder-treated animals. Thus, LCB1v1.3 is effective against historical and circulating SARS-CoV-2, as well as strains encoding mutations of concern.

DISCUSSION

Here, using the stringent K18-hACE2 mouse model of SARS-CoV-2 pathogenesis, we show that LCB1-Fc, an Fc-containing

Please cite this article in press as: Case et al., Ultrapotent miniproteins targeting the SARS-CoV-2 receptor-binding domain protect against infection and disease, Cell Host & Microbe (2021), https://doi.org/10.1016/j.chom.2021.06.008

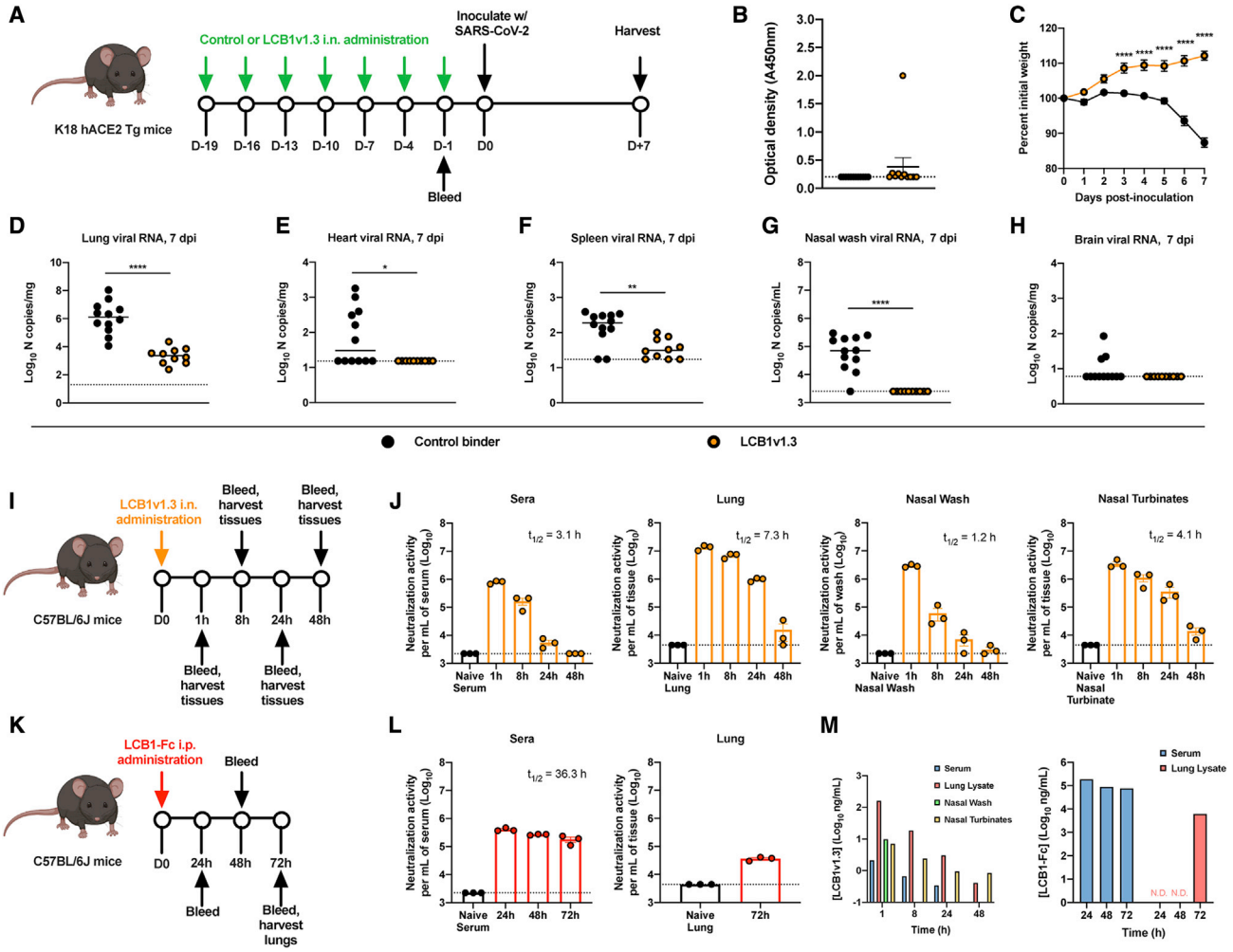

Figure 5. Immunogenicity and functional pharmacokinetic properties of SARS-CoV-2 RBD miniproteins

(A) Scheme of experimental details. K18-hACE2 transgenic mice (n = 10–12 per group) were treated every 3 days with 50 μg of LCB1v1.3 or control binder by i.n. administration. On day 18 post-treatment, animals were bled and anti-LCB1v1.3 antibodies were measured. The following day, animals were challenged with 10^3 PFU of SARS-CoV-2, and tissues were collected at 7 dpi.

(B) Binding of serum antibodies to LCB1v1.3 as measured by ELISA (mean ± SEM, three experiments). Dashed line indicated limit of detection of the assay.

(C) Weight change following LCB1v1.3 or control binder administration (mean ± SEM; two experiments: two-way ANOVA with Sidak's post-test: ****$p < 0.0001$).

(D–H) Viral RNA levels at 7 dpi in the lung, heart, spleen, brain, or nasal wash (two experiments: Mann-Whitney test: *$p < 0.05$, **$p < 0.01$, ****$p < 0.0001$).

(I–M) C57BL/6J mice were treated with 200 μg of LCB1v1.3 by i.n. administration or 250 μg of LCB1-Fc by i.p. injection. At the indicated times post-administration, animals were bled and tissues collected (LCB1v1.3) or harvested after the final bleed (LCB1-Fc) (I and K). The levels of neutralizing activity in serum, lung homogenate, nasal wash, and nasal turbinate homogenate from LCB1v1.3-treated animals or serum and lung homogenate from LCB1-Fc-treated animals were determined by FRNT (J and L) or ELISA (M).

Data are represented as the neutralizing activity ($1/EC_{50}$ value) per mL or binder concentration present in each sample at each collection time (n = 3 animals per group, one experiment, N.D., not determined).

version of a previously reported SARS-CoV-2 RBD binding miniprotein, LCB1 (Cao et al., 2020), prevented SARS-CoV-2 infection and disease when administered 1 day before or after virus inoculation. Lung biomechanics of K18-hACE2 mice treated with LCB1-Fc mirrored those of naive animals in all parameters tested. We corroborated our findings of virological protection with LCB1-Fc in a separate 129S2 mouse model of infection.

We also evaluated the efficacy of LCB1v1.3, an optimized, monomeric form of LCB1 without an Fc domain. A single i.n. dose of LCB1v1.3 reduced viral burden when administered as many as 5 days before or 2 days after SARS-CoV-2 infection. While several antibody-based intravenous therapies have been developed against SARS-CoV-2, our approach of using ultrapotent *de novo*-designed minibinders for i.n. delivery is unique. The closest comparator is the i.n. delivery of a multivalent three-domain anti-RBD camelid nanobody daisy chain (PiN-21), which protects Syrian hamsters from weight loss and reduces viral burden when administered 6 h after SARS-CoV-2 infection (Nambulli et al., 2021). I.n. type I interferon therapy for SARS-CoV-2 also was reported in a hamster model of disease (Hoagland et al., 2021), but with limited efficacy.

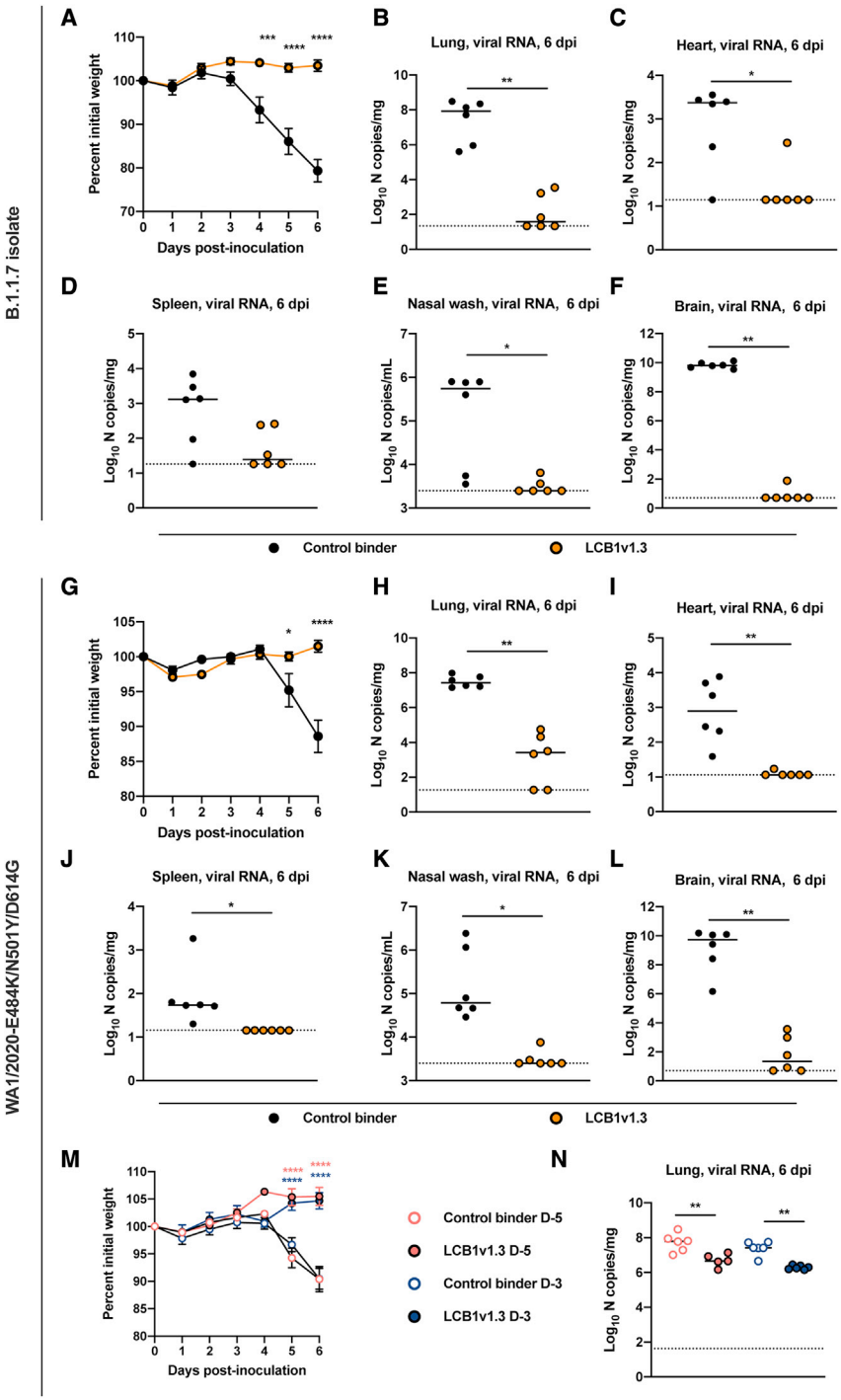

Figure 6. LCB1v1.3 protects mice against B.1.1.7 variant and WA1/2020 E484K/N501Y/D614G strains

(A–F) 7- to 8-week-old female K18-hACE2 mice were treated with a single 50-μg i.n. dose of LCB1v1.3 or control binder at 1 day prior to i.n. inoculation with 10^3 PFU of B.1.1.7. (A) Weight change following LCB1v1.3 or control binder administration (mean ± SEM; n = 6, two experiments: two-way ANOVA with Sidak's post-test: ***$p < 0.001$, ****$p < 0.0001$). (B–F) Viral RNA levels at 6 dpi in the lung, heart, spleen, nasal wash, or brain (n = 6, two experiments: Mann-Whitney test: *$p < 0.05$, **$p < 0.01$).

(G–L) 8-week-old male K18-hACE2 transgenic mice were treated with a single 50-μg i.n. dose of LCB1v1.3 or control binder at 1 day prior to i.n. inoculation with 10^3 PFU of WA1/2020-E484K/N501Y/D614G. (G) Weight change following LCB1v1.3 or control binder administration (mean ± SEM; n = 6, two experiments: two-way ANOVA with Sidak's post-test: *$p < 0.05$, ****$p < 0.0001$). (H–L) Viral RNA levels at 6 dpi in the lung, heart, spleen, nasal wash, or brain (n = 6, two experiments: Mann-Whitney test: *$p < 0.05$, **$p < 0.01$).

(M and N) 7- to 8-week-old female K18-hACE2 mice received a single 50-μg dose of LCB1v1.3 or control binder via the i.n. route at the indicated time prior to i.n. inoculation with 10^3 PFU of WA1/2020-E484K/N501Y/D614G. (M) Weight change following LCB1v1.3 or control binder administration (mean ± SEM; n = 5–6, two experiments: two-way ANOVA with Sidak's post-test: ****$p < 0.0001$). (N) Lung tissues were collected at 6 dpi and viral RNA levels were determined (n = 5–6 animals per group, two-experiments: Mann-Whitney test: **$p < 0.01$).

See also Figure S6.

The K18-hACE2 mouse model recapitulates several aspects of severe COVID-19, including lung inflammation and reduced pulmonary function (Golden et al., 2020; Winkler et al., 2020). Since K18-hACE2 mice are highly vulnerable to infection, the therapeutic window of treatment is limited (Winkler et al., 2021). Despite this, LCB1-Fc treatment begun at D+2 or D+3 conferred 100% survival after a lethal dose challenge of SARS-CoV-2. Furthermore, LCB1-Fc or LCB1v1.3 binder treatment before or after infection limited immune cell infiltration and lung inflammation, which prevented tissue damage and compromise of respiratory function. Although formal pharmacokinetics, safety, and toxicology studies are needed for our miniprotein prior to clinical studies, our functional analyses suggest that the half-life of LCB1v1.3 in the respiratory tract is approximately 6–12 h, and prophylactic doses of as low as 0.1 mg/kg confer protection. In comparison, LCB1-Fc, which likely does not accumulate to high levels in the upper respiratory tract (Reynolds, 1988), has a longer half-life in circulation because of its Fc domain and ability to engage the neonatal Fc receptor (Challa et al., 2014). Although our *in vivo* studies with LCB1v1.3, which lacks an Fc domain, suggest that our miniprotein binders confer protection through their neutralizing activity, engagement of complement and FcγRs could augment the therapeutic activity of LCB1-Fc, as described recently with anti-SARS-CoV-2 monoclonal antibodies (Schäfer et al., 2021; Winkler et al., 2021). These functions could be explored using loss-of-Fc-function (e.g., LALA-PG) variants of LCB1-Fc. Depending on the outcome, Fc effector functions could be

Please cite this article in press as: Case et al., Ultrapotent miniproteins targeting the SARS-CoV-2 receptor-binding domain protect against infection and disease, Cell Host & Microbe (2021), https://doi.org/10.1016/j.chom.2021.06.008

optimized further through glycan modification or Fc mutation (Kang and Jung, 2019). While we observed reductions in lung viral burden from a single i.n. dose of LCB1v1.3 given 2 days after virus inoculation, it will be important to improve upon this result. Possible ways to achieve this include higher dosing, repeated dosing, or extended half-life engineering. As part of our proof-of-principle studies for a nasal prophylaxis, we observed little immunogenicity of LCB1v1.3, suggesting that repeated dosing may be possible. Evaluation of miniprotein binders in hamsters and NHPs is needed to extend the efficacy data and provide further rationale for human clinical trials.

Although several antibody-based therapies demonstrate promise against SARS-CoV-2 and a few have been granted EUA status, viral evolution could jeopardize these interventions, especially in the context of emerging variants (e.g., B.1.1.7, B.1.351, B.1.1.28, and B.1.617.2). Indeed, we and others have observed that many monoclonal and polyclonal antibodies showed reduced neutralization activity against several of these variant strains (Chen et al., 2021; Wang et al., 2021a, 2021b; Wibmer et al., 2021; Xie et al., 2021). In comparison, LCB1v1.3 showed efficacy against historical (WA1/2020) and emerging (B.1.1.7 and E484K/N501Y/D614G) SARS-CoV-2 strains. Based on the cryoelectron microscopy (cryo-EM) structure of the parent LCB1 binder in complex with SARS-CoV-2 RBD (Cao et al., 2020), only the N501Y mutation is expected to affect binding. While we observed a decrease in the neutralizing activity of LCB1v1.3 against the emerging variants, EC_{50} values were still less than 800 pM, suggesting that substantial potency was retained. Additional optimization of LCB1-Fc- and LCB1v1.3-RBD binding interactions, through computational design and functional validation, could reduce the effects of variant mutations on neutralizing activity. Moreover, the development of binder combinations that target different regions of the spike protein of multiple emerging SARS-CoV-2 variants is planned.

Compared to other potential SARS-CoV-2 antibody-based treatments, miniproteins have several benefits: (1) due to their smaller size, they can bind each protomer of a single trimeric spike, resulting in greater potency for a given dose; (2) they can be manufactured cost effectively; (3) if warranted, they can be refined to overcome escape by new SARS-CoV-2 variants; and (4) they can be mixed using linker proteins to generate multimerized constructs that limit resistance. In summary, our data highlight the promise of rational antiviral protein design and support the development of LCB1v1.3 and LCB1-Fc as potent SARS-CoV-2-specific countermeasures.

Limitations of study

In this study, we established the efficacy of two lead candidate miniproteins, LCB1-Fc and LCB1v1.3, against SARS-CoV-2 in K18-hACE2 and 129S2 mice, which have severe and moderate disease phenotypes, respectively. We acknowledge that the therapeutic activity of the miniproteins will need to be corroborated in additional relevant animal models, such as hamsters and non-human primates. Indeed, the immunogenicity and pharmacokinetic and pharmacodynamic properties of the minibinders in larger vertebrate animals will inform possible clinical evaluation in humans. The half-life studies of LCB1-Fc should be performed for longer durations, potentially yielding greater half-life resolution. Moreover, although our pharmacokinetic studies determined the absolute and functional concentrations of minibinders present in key tissues, whole-mouse biodistribution studies with fluorescently labeled binders are planned. We performed immunogenicity studies only with LCB1v1.3, and thus, LCB1-Fc will need similar assessment. We evaluated the immunogenicity of LCB1v1.3 using repeated dosing every 3 days for a total of 18 days and observed that only one of ten animals developed antibodies against LCB1v1.3. While we interpreted this result as a lack of immunogenicity, it is possible that we induced immune tolerance against the binder. Additional immunogenicity experiments are warranted that include different dosing schedules, a range of dosing concentrations, and longer time points of observation.

Over the past several months, variants of concern have emerged and become dominantly circulating strains. Treatment with LCB1v1.3 conferred high levels of protection against a B.1.1.7 isolate and a recombinant WA1/2020 strain encoding N501Y/E484K/D614G mutations. We acknowledge that while mutations at positions N501 and E484 confer resistance to a number of clinically advanced monoclonal and vaccine-induced antibodies (Chen et al., 2021; Wang et al., 2021a, 2021b; Wibmer et al., 2021), they do not encompass all antigenic properties of the B.1.351 and B.1.1.28 spike proteins. Because structural data suggested that the N501Y mutation might affect LCB1 binding (Cao et al., 2020), we tested LCB1v1.3 against a virus encoding this mutation *in vivo*. Nonetheless, studies that test LCB1-Fc and LCB1v1.3 efficacy against additional SARS-CoV-2 variants of concern are planned and important for further product development.

STAR★METHODS

Detailed methods are provided in the online version of this paper and include the following:

- KEY RESOURCES TABLE
- RESOURCE AVAILABILITY
  - Lead contact
  - Materials availability
  - Data and code availability
- EXPERIMENTAL MODEL AND SUBJECT DETAILS
  - Cells and viruses
  - Mouse experiments
- METHOD DETAILS
  - Miniprotein production
  - Biolayer interferometry
  - Plaque assay
  - Measurement of viral burden
  - Cytokine and chemokine mRNA measurements
  - Lung pathology
  - Respiratory mechanics
  - Neutralization assay
  - ELISA
- QUANTIFICATION AND STATISTICAL ANALYSIS

SUPPLEMENTAL INFORMATION

Supplemental information can be found online at https://doi.org/10.1016/j.chom.2021.06.008.

ACKNOWLEDGMENTS

This study was supported by NIH grants (R01 AI157155, AI134907, and UL1TR001439), the Defense Advanced Research Project Agency (HR001117S0019 and HR0011835403 contract FA8750-17-C-0219), the Audacious Project at the Institute for Protein Design (L. Carter and D.B.), funding from E. and W. Schmidt by recommendation of the Schmidt Futures program (L. Carter, R.R., I.G., and D.B.), the Open Philanthropy Project Improving Protein Design Fund (D.B.), Bill and Melinda Gates Foundation #OPP1156262 (L.S., L. Carter, M.N.P., R.R., and D.B.), and a gift from the Granieri family (M.J.). J.B.C. is supported by a Helen Hay Whitney Foundation postdoctoral fellowship, E.S.W. is supported by F30 AI152327, N.M.K. is supported by T32 AI007172, and P.-Y.S. is supported by awards from the Sealy and Smith Foundation, the Kleberg Foundation, the John S. Dunn Foundation, the Amon G. Carter Foundation, the Gilson Longenbaugh Foundation, and the Summerfield Robert Foundation. We thank Lisa Kozodoy and Lexi Walls for support in development of ELISA assays; Cassie Ogohara and Michael Murphy for support in protein production and purification; the Pulmonary Morphology Core at Washington University School of Medicine for tissue sectioning and slide preparation; and SCIREQ Inc. for providing the flexiVent pulmonary mechanics research platform and analysis software.

AUTHOR CONTRIBUTIONS

J.B.C., L.S., D.B., and M.S.D. designed the research. J.B.C., R.E.C., E.S.W., S.S., and N.M.K. performed mouse experiments and clinical analyses. J.B.C. and B.Y. performed viral burden analysis. J.B.C. and E.S.W. performed pulmonary mechanics analysis. A.L.B. analyzed the tissue sections for histopathology. J.B.C. and R.E.C. performed neutralization analysis. L. Cao optimized protein designs, generated computational models, and performed BLI analysis. L. Carter and R.R. purified and prepared the miniproteins. M.J., M.N.P., I.G., and L.S. developed and performed ELISA analysis. X.X. and P.-Y.S. provided the recombinant virus strains. J.B.C. and M.S.D. wrote the initial draft, with other authors providing editorial comments and helpful discussions about the research.

DECLARATION OF INTERESTS

M.S.D. is a consultant for Inbios, Vir Biotechnology, Fortress Biotech, and Carnival Corporation, and is on the scientific advisory boards of Moderna and Immunome. The Diamond laboratory has received unrelated funding support in sponsored research agreements from Moderna, Vir Biotechnology, and Emergent BioSolutions. L. Cao, I.G., L.S., J.B.C., M.S.D., and D.B. are coinventors on a provisional patent application that incorporates discoveries described in this manuscript. D.B. is a cofounder of Neoleukin Therapeutics.

Received: March 9, 2021
Revised: May 23, 2021
Accepted: June 11, 2021
Published: June 24, 2021

REFERENCES

Cao, L., Goreshnik, I., Coventry, B., Case, J.B., Miller, L., Kozodoy, L., Chen, R.E., Carter, L., Walls, A.C., Park, Y.J., et al. (2020). De novo design of picomolar SARS-CoV-2 miniprotein inhibitors. Science *370*, 426–431.

Case, J.B., Bailey, A.L., Kim, A.S., Chen, R.E., and Diamond, M.S. (2020). Growth, detection, quantification, and inactivation of SARS-CoV-2. Virology *548*, 39–48.

Challa, D.K., Velmurugan, R., Ober, R.J., and Sally Ward, E. (2014). FcRn: from molecular interactions to regulation of IgG pharmacokinetics and functions. Curr. Top. Microbiol. Immunol. *382*, 249–272.

Chen, R.E., Zhang, X., Case, J.B., Winkler, E.S., Liu, Y., VanBlargan, L.A., Liu, J., Errico, J.M., Xie, X., Suryadevara, N., et al. (2021). Resistance of SARS-CoV-2 variants to neutralization by monoclonal and serum-derived polyclonal antibodies. Nat. Med. *27*, 717–726.

Chevalier, A., Silva, D.A., Rocklin, G.J., Hicks, D.R., Vergara, R., Murapa, P., Bernard, S.M., Zhang, L., Lam, K.H., Yao, G., et al. (2017). Massively parallel de novo protein design for targeted therapeutics. Nature *550*, 74–79.

Day, M. (2020). Covid-19: identifying and isolating asymptomatic people helped eliminate virus in Italian village. BMJ *368*, m1165.

Galloway, S.E., Paul, P., MacCannell, D.R., Johansson, M.A., Brooks, J.T., MacNeil, A., Slayton, R.B., Tong, S., Silk, B.J., Armstrong, G.L., et al. (2021). Emergence of SARS-CoV-2 B.1.1.7 Lineage - United States, December 29, 2020-January 12, 2021. MMWR Morb. Mortal. Wkly. Rep. *70*, 95–99.

Golden, J.W., Cline, C.R., Zeng, X., Garrison, A.R., Carey, B.D., Mucker, E.M., White, L.E., Shamblin, J.D., Brocato, R.L., Liu, J., et al. (2020). Human angiotensin-converting enzyme 2 transgenic mice infected with SARS-CoV-2 develop severe and fatal respiratory disease. JCI Insight. https://doi.org/10.1172/jci.insight.142032.

Gu, H., Chen, Q., Yang, G., He, L., Fan, H., Deng, Y.Q., Wang, Y., Teng, Y., Zhao, Z., Cui, Y., et al. (2020). Adaptation of SARS-CoV-2 in BALB/c mice for testing vaccine efficacy. Science *369*, 1603–1607.

Hassan, A.O., Case, J.B., Winkler, E.S., Thackray, L.B., Kafai, N.M., Bailey, A.L., McCune, B.T., Fox, J.M., Chen, R.E., Alsoussi, W.B., et al. (2020). A SARS-CoV-2 Infection Model in Mice Demonstrates Protection by Neutralizing Antibodies. Cell *182*, 744–753.e4.

Hoagland, D.A., Møller, R., Uhl, S.A., Oishi, K., Frere, J., Golynker, I., Horiuchi, S., Panis, M., Blanco-Melo, D., Sachs, D., et al. (2021). Leveraging the antiviral type I interferon system as a first line of defense against SARS-CoV-2 pathogenicity. Immunity *54*, 557–570.e5.

Hoffmann, M., Kleine-Weber, H., Schroeder, S., Krüger, N., Herrler, T., Erichsen, S., Schiergens, T.S., Herrler, G., Wu, N.H., Nitsche, A., et al. (2020). SARS-CoV-2 Cell Entry Depends on ACE2 and TMPRSS2 and Is Blocked by a Clinically Proven Protease Inhibitor. Cell *181*, 271–280.e8.

Jeyanathan, M., Afkhami, S., Smaill, F., Miller, M.S., Lichty, B.D., and Xing, Z. (2020). Immunological considerations for COVID-19 vaccine strategies. Nat. Rev. Immunol. *20*, 615–632.

Johnson, K.D., Harris, C., Cain, J.K., Hummer, C., Goyal, H., and Perisetti, A. (2020). Pulmonary and Extra-Pulmonary Clinical Manifestations of COVID-19. Front. Med. (Lausanne) *7*, 526.

Kang, T.H., and Jung, S.T. (2019). Boosting therapeutic potency of antibodies by taming Fc domain functions. Exp. Mol. Med. *51*, 1–9.

Kordzadeh-Kermani, E., Khalili, H., and Karimzadeh, I. (2020). Pathogenesis, clinical manifestations and complications of coronavirus disease 2019 (COVID-19). Future Microbiol. *15*, 1287–1305.

Krammer, F. (2020). SARS-CoV-2 vaccines in development. Nature *586*, 516–527.

Letko, M., Marzi, A., and Munster, V. (2020). Functional assessment of cell entry and receptor usage for SARS-CoV-2 and other lineage B betacoronaviruses. Nat. Microbiol. *5*, 562–569.

Leung, K., Shum, M.H., Leung, G.M., Lam, T.T., and Wu, J.T. (2021). Early transmissibility assessment of the N501Y mutant strains of SARS-CoV-2 in the United Kingdom, October to November 2020. Euro Surveill. https://doi.org/10.2807/1560-7917.ES.2020.26.1.2002106.

Li, R., Pei, S., Chen, B., Song, Y., Zhang, T., Yang, W., and Shaman, J. (2020). Substantial undocumented infection facilitates the rapid dissemination of novel coronavirus (SARS-CoV-2). Science *368*, 489–493.

Matsuyama, S., Nao, N., Shirato, K., Kawase, M., Saito, S., Takayama, I., Nagata, N., Sekizuka, T., Katoh, H., Kato, F., et al. (2020). Enhanced isolation of SARS-CoV-2 by TMPRSS2-expressing cells. Proc. Natl. Acad. Sci. USA *117*, 7001–7003.

McGovern, T.K., Robichaud, A., Fereydoonzad, L., Schuessler, T.F., and Martin, J.G. (2013). Evaluation of respiratory system mechanics in mice using the forced oscillation technique. J. Vis. Exp. https://doi.org/10.3791/50172.

Mukherjee, S., Sirohi, D., Dowd, K.A., Chen, Z., Diamond, M.S., Kuhn, R.J., and Pierson, T.C. (2016). Enhancing dengue virus maturation using a stable furin over-expressing cell line. Virology *497*, 33–40.

Nambulli, S., Xiang, Y., Tilston-Lunel, N.L., Rennick, L.J., Sang, Z., Klimstra, W.B., Reed, D.S., Crossland, N.A., Shi, Y., and Duprex, W.P. (2021). Inhalable Nanobody (PiN-21) prevents and treats SARS-CoV-2 infections in Syrian hamsters at ultra-low doses. bioRxiv. https://doi.org/10.1126/sciadv.abh0319.

Petersen, E., Koopmans, M., Go, U., Hamer, D.H., Petrosillo, N., Castelli, F., Storgaard, M., Al Khalili, S., and Simonsen, L. (2020). Comparing SARS-CoV-2 with SARS-CoV and influenza pandemics. Lancet Infect. Dis. *20*, e238–e244.

Rathnasinghe, R., Jangra, S., Cupic, A., Martinez-Romero, C., Mulder, L.C.F., Kehrer, T., Yildiz, S., Choi, A., Mena, I., De Vrieze, J., et al. (2021). The N501Y mutation in SARS-CoV-2 spike leads to morbidity in obese and aged mice and is neutralized by convalescent and post-vaccination human sera. medRxiv. https://doi.org/10.1101/2021.01.19.21249592.

Reynolds, H.Y. (1988). Immunoglobulin G and its function in the human respiratory tract. Mayo Clin. Proc. *63*, 161–174.

Schäfer, A., Muecksch, F., Lorenzi, J.C.C., Leist, S.R., Cipolla, M., Bournazos, S., Schmidt, F., Maison, R.M., Gazumyan, A., Martinez, D.R., et al. (2021). Antibody potency, effector function, and combinations in protection and therapy for SARS-CoV-2 infection in vivo. J. Exp. Med. https://doi.org/10.1084/jem.20201993.

Tegally, H., Wilkinson, E., Giovanetti, M., Iranzadeh, A., Fonseca, V., Giandhari, J., Doolabh, D., Pillay, S., San, E.J., Msomi, N., et al. (2020). Emergence and rapid spread of a new severe acute respiratory syndrome-related coronavirus 2 (SARS-CoV-2) lineage with multiple spike mutations in South Africa. medRxiv. https://doi.org/10.1101/2020.12.21.20248640.

VanBlargan, L.A., Adams, L.J., Liu, Z., Chen, R.E., Gilchuk, P., Raju, S., Smith, B.K., Zhao, H., Case, J.B., Winkler, E.S., et al. (2021). A potently neutralizing anti-SARS-CoV-2 antibody inhibits variants of concern by binding a highly conserved epitope. bioRxiv. https://doi.org/10.1101/2021.04.26.441501.

Voloch, C.M., da Silva Francisco, R., Jr., de Almeida, L.G.P., Cardoso, C.C., Brustolini, O.J., Gerber, A.L., Guimarães, A.P.C., Mariani, D., da Costa, R.M., Ferreira, O.C., Jr., et al.; Covid19-UFRJ Workgroup, LNCC Workgroup, Adriana Cony Cavalcanti (2021). Genomic characterization of a novel SARS-CoV-2 lineage from Rio de Janeiro, Brazil. J. Virol. *95*, e00119–e00121.

Wang, P., Nair, M.S., Liu, L., Iketani, S., Luo, Y., Guo, Y., Wang, M., Yu, J., Zhang, B., Kwong, P.D., et al. (2021a). Antibody resistance of SARS-CoV-2 variants B.1.351 and B.1.1.7. Nature *593*, 130–135.

Wang, Z., Schmidt, F., Weisblum, Y., Muecksch, F., Barnes, C.O., Finkin, S., Schaefer-Babajew, D., Cipolla, M., Gaebler, C., Lieberman, J.A., et al. (2021b). mRNA vaccine-elicited antibodies to SARS-CoV-2 and circulating variants. Nature *592*, 616–622.

Wibmer, C.K., Ayres, F., Hermanus, T., Madzivhandila, M., Kgagudi, P., Oosthuysen, B., Lambson, B.E., de Oliveira, T., Vermeulen, M., van der Berg, K., et al. (2021). SARS-CoV-2 501Y.V2 escapes neutralization by South African COVID-19 donor plasma. Nat. Med. *27*, 622–625.

Winkler, E.S., Bailey, A.L., Kafai, N.M., Nair, S., McCune, B.T., Yu, J., Fox, J.M., Chen, R.E., Earnest, J.T., Keeler, S.P., et al. (2020). SARS-CoV-2 infection of human ACE2-transgenic mice causes severe lung inflammation and impaired function. Nat. Immunol. *21*, 1327–1335.

Winkler, E.S., Gilchuk, P., Yu, J., Bailey, A.L., Chen, R.E., Chong, Z., Zost, S.J., Jang, H., Huang, Y., Allen, J.D., et al. (2021). Human neutralizing antibodies against SARS-CoV-2 require intact Fc effector functions for optimal therapeutic protection. Cell *184*, 1804–1820.e16.

Xie, X., Liu, Y., Liu, J., Zhang, X., Zou, J., Fontes-Garfias, C.R., Xia, H., Swanson, K.A., Cutler, M., Cooper, D., et al. (2021). Neutralization of SARS-CoV-2 spike 69/70 deletion, E484K and N501Y variants by BNT162b2 vaccine-elicited sera. Nat. Med. *27*, 620–621.

Zhou, F., Yu, T., Du, R., Fan, G., Liu, Y., Liu, Z., Xiang, J., Wang, Y., Song, B., Gu, X., et al. (2020). Clinical course and risk factors for mortality of adult inpatients with COVID-19 in Wuhan, China: a retrospective cohort study. Lancet *395*, 1054–1062.

Zhou, D., Chan, J.F.-W., Zhou, B., Zhou, R., Li, S., Shan, S., Liu, L., Zhang, A.J., Chen, S.J., Chan, C.C.-S., et al. (2021). Robust SARS-CoV-2 infection in nasal turbinates after treatment with systemic neutralizing antibodies. Cell Host Microbe *29*, 551–563.e5.

Please cite this article in press as: Case et al., Ultrapotent miniproteins targeting the SARS-CoV-2 receptor-binding domain protect against infection and disease, Cell Host & Microbe (2021), https://doi.org/10.1016/j.chom.2021.06.008

STAR★METHODS

KEY RESOURCES TABLE

REAGENT or RESOURCE	SOURCE	IDENTIFIER
Antibodies		
Anti-mouse IgG peroxidase	Sigma-Aldrich	Cat# A8924-5mL; RRID:AB_258426
Anti-spike oligoclonal pool	VanBlargan et al., 2021	N/A
Anti-human IgG peroxidase	Invitrogen	Cat# 05-4220 RRID:AB_2532922
Anti-human IgG peroxidase	Invitrogen	Cat# A18817 RRID:AB_2535594
Anti-mouse IgG peroxidase	Vector Laboratories	Cat# PI-2000-1 RRID:AB_2313581
Bacterial and virus strains		
2019 n-CoV/USA_WA1/2020	BEI	Cat# NR-52281
B.1.1.7	Chen et al., 2021	N/A
WA1/2020-N501Y/D614G	Xie et al., 2021	N/A
WA1/2020-E484K/N501Y/D614G	Xie et al., 2021	N/A
Chemicals, peptides, and recombinant proteins		
TrueBlue peroxidase substrate	KPL/SeraCare	Cat# 5510-0050
Critical commercial assays		
MagMAX mirVana Total RNA Isolation Kit	Thermo Fisher	A27828
TaqMan RNA-to-Ct 1-Step Kit	Thermo Fisher	4392939
Ambion DNase I (RNase-free)	Thermo Fisher	AM2222
High-Capacity cDNA Reverse Transcription Kit with RNase Inhibitor	Thermo Fisher	4374966
TaqMan Fast Universal PCR Mix, No AmpErase	Thermo Fisher	4352042
Experimental models: Cell lines		
Vero CCL81	ATCC	Cat# CCL-81: RRID:CVCL_0059
Vero E6	ATCC	Cat# CRL-1586: RRID:CVCL_0574
Vero-furin	Mukherjee et al., 2016	N/A
Vero-hACE2-TMPRSS2	A. Creanga and B. Graham	N/A
Expi293F	Thermo Fisher	Cat# A14527
Experimental models: Organisms/strains		
Mouse: B6.Cg-Tg(K18-ACE2)2Prlmn/J	Jackson Laboratory	Cat# 034860; IMSR_JAX:034860
Mouse: C57BL/6J	Jackson Laboratory	Cat# 000664
Mouse: 129S2 (SvPasCrl)	Charles River Laboratories	Strain code: 476; IMSR_CRL:129S2/SvPasCrl(Elite)
Oligonucleotides		
SARS-CoV-2 N **F**: 5′-ATGCTGCA ATCGTGCTACAA-3′	Hassan et al., 2020	N/A
SARS-CoV-2 N **R**: 5′-GACTGCCGCCTCTGCTC-3′	Hassan et al., 2020	N/A
SARS-CoV-2 N **Probe**: 5′-/56-FAM/TCAAGGA AC/ZEN/ AACATTGCCAA/3IABkFQ/-3′	Hassan et al., 2020	N/A
Gapdh TaqMan Primer/Probe set	IDT	Mm.PT.39a.1
Ifng TaqMan Primer/Probe set	IDT	Mm.PT.58.41769240
Il6 TaqMan Primer/Probe set	IDT	Mm.PT.58.10005566
Il1b TaqMan Primer/Probe set	IDT	Mm.PT.58.41616450
Tnfa TaqMan Primer/Probe set	IDT	Mm.PT.58.12575861
Cxcl10 TaqMan Primer/Probe set	IDT	Mm.PT.58.43575827
Cxcl11 TaqMan Primer/Probe set	IDT	Mm.PT.58.10773148.g

(*Continued on next page*)

Continued

REAGENT or RESOURCE	SOURCE	IDENTIFIER
Ifnb TaqMan Primer/Probe set	IDT	Mm.PT.58.30132453.g
CXCL1 TaqMan Primer/Probe set	IDT	Mm.PT.58.42076891
Ccl2 TaqMan Primer/Probe set	IDT	Mm.PT.58.42151692
Ccl5 TaqMan Primer/Probe set	IDT	Mm.PT.58.43548565
Recombinant DNA		
pCMVR	GenScript	N/A
pet29b	GenScript	N/A
Software and algorithms		
BioRender	Biorender.com	N/A
flexiWare	SCIREQ Inc.	v8.1.3
Nanozoomer Digital Pathology	Hamamatsu	v2
Statistics: Prism 9.0	GraphPad	N/A

RESOURCE AVAILABILITY

Lead contact

Further information and requests for resources and reagents should be directed to the Lead Contact, Michael S. Diamond (diamond@wusm.wustl.edu).

Materials availability

All requests for resources and reagents should be directed to the Lead Contact author. This includes mice, antibodies, protein mini-binders, and viruses. All reagents will be made available on request after completion of a Materials Transfer Agreement.

Data and code availability

All data supporting the findings of this study are available within the paper and are available from the corresponding author upon request.

EXPERIMENTAL MODEL AND SUBJECT DETAILS

Cells and viruses

Vero E6 (CRL-1586, American Type Culture Collection (ATCC), Vero CCL81 (ATCC), Vero-furin (Mukherjee et al., 2016), and Vero-hACE2-TMPRSS2 (a gift of A. Creanga and B. Graham, NIH) were cultured at 37°C in Dulbecco's Modified Eagle medium (DMEM) supplemented with 10% fetal bovine serum (FBS), 10 mM HEPES pH 7.3, 1 mM sodium pyruvate, 1 × non-essential amino acids, and 100 U/mL of penicillin–streptomycin. Additionally, Vero-TMPRSS2 and Vero-hACE2-TMPRSS2 cells were cultured in the presence of 5 μg/mL of blasticidin or puromycin, respectively. The WA1/202 (2019n-CoV/USA_WA1/2020) isolate of SARS-CoV-2 was obtained from the US Centers for Disease Control (CDC). The B.1.1.7, WA1/2020-N501Y/D614G, and WA1/2020-E484K/N501Y/D614G viruses have been described previously (Chen et al., 2021; Xie et al., 2021). Infectious stocks were propagated by inoculating Vero CCL81 or Vero-hACE2-TMPRSS2 cells. Supernatant was collected, aliquoted, and stored at −80°C. All work with infectious SARS-CoV-2 was performed in Institutional Biosafety Committee-approved BSL3 and A-BSL3 facilities at Washington University School of Medicine using positive pressure air respirators and protective equipment. All virus stocks were deep-sequenced after RNA extraction to confirm the presence of the anticipated substitutions.

Mouse experiments

Animal studies were carried out in accordance with the recommendations in the Guide for the Care and Use of Laboratory Animals of the National Institutes of Health. The protocols were approved by the Institutional Animal Care and Use Committee at the Washington University School of Medicine (assurance number A3381–01). Virus inoculations were performed under anesthesia that was induced and maintained with ketamine hydrochloride and xylazine, and all efforts were made to minimize animal suffering.

Heterozygous K18-hACE C57BL/6J mice (strain: 2B6.Cg-Tg(K18-ACE2)2Prlmn/J) and C57BL/6J mice (strain: 000664) were obtained from The Jackson Laboratory and 129S2 mice (strain: 129S2/SvPasCrl) from Charles River Laboratories. Animals were housed in groups and fed standard chow diets. Mice of different ages and both sexes were administered 10^3 PFU of SARS-CoV-2 via intranasal administration.

Please cite this article in press as: Case et al., Ultrapotent miniproteins targeting the SARS-CoV-2 receptor-binding domain protect against infection and disease, Cell Host & Microbe (2021), https://doi.org/10.1016/j.chom.2021.06.008

METHOD DETAILS

Miniprotein production

LCB1-Fc was synthesized and cloned by GenScript into pCMVR plasmid, with kanamycin resistance. Plasmids were transformed into the NEB 5-alpha strain of *E. coli* (New England Biolabs) to recover DNA for transient transfection into Expi293F mammalian cells. Expi293F cells were grown in suspension using Expi293F expression medium (Life Technologies) at 33°C, 70% humidity, and 8% CO_2 rotating at 150 rpm. The cultures were transfected using PEI-MAX (Polyscience) with cells grown to a density of 3×10^6 cells per mL and cultivated for 3 days. Supernatants were clarified by centrifugation (5 min at 4000 x *g*, addition of PDADMAC solution to a final concentration of 0.0375% (Sigma Aldrich, #409014), and a second spin (5 min at 4000 x *g*). Clarified supernatants were purified using a MabSelect PrismA 2.6 × 5 cm column (Cytiva) on an AKTA Avant150 FPLC (Cytiva). Bound protein was washed with five column volumes of 20 mM $NaPO_4$ and 150 mM NaCl pH 7.2, then five column volumes of 20 mM $NaPO_4$ and 1 M NaCl pH 7.4, and eluted with three column volumes of 100 mM glycine at pH 3.0. The eluate was neutralized with 2 M Tris base to a final concentration of 50 mM. SDS-PAGE was used to assess protein purity. The protein was passed through a 0.22 μm filter and stored at 4°C until use.

LCB1v1.3 with polar mutations (4N, 14K, 15T, 17E, 18Q, 27Q, 38Q) relative to the original LCB1 was cloned into a pet29b vector. LCB1v1.3 was expressed in Lemo21(DE3) (NEB) in terrific broth media and grown in 2 L baffled shake flasks. Bacteria were propagated at 37°C to an O.D.600 of ~0.8, and then induced with 1 mM IPTG. Expression temperature was reduced to 18°C, and the cells were shaken for ~16 h. The cells were harvested and lysed using heat treatment and incubated at 80°C for 10 min with stirring. Lysates were clarified by centrifugation at 24,000 × *g* for 30 min and applied to a 2.6 × 10 cm Ni Sepharose 6 FF column (Cytiva) for purification by IMAC on an AKTA Avant150 FPLC system (Cytiva). Proteins were eluted over a linear gradient of 30 mM to 500 mM imidazole in a buffer of 50 mM Tris pH 8.0 and 500 mM NaCl. Peak fractions were pooled, concentrated in 10 kDa MWCO centrifugal filters (Millipore), sterile filtered (0.22 μm) and applied to either a Superdex 200 Increase 10/300, or HiLoad S200 pg GL SEC column (Cytiva) using 50 mM phosphate pH 7.4, 150 mM NaCl buffer. After size exclusion chromatography, bacterial-derived components were tested to confirm low levels of endotoxin.

Biolayer interferometry

Biolayer interferometry data were collected using an Octet RED96 (ForteBio) and processed using the instrument's integrated software. Briefly, biotinylated RBD (Acro Biosystems) was loaded onto streptavidin-coated biosensors (SA ForteBio) at 20 nM in binding buffer (10 mM HEPES (pH 7.4), 150 mM NaCl, 3 mM EDTA, 0.05% surfactant P20, and 0.5% non-fat dry milk) for 360 s. Analyte proteins (LCB1v1.3 or LCB1-Fc) were diluted from concentrated stocks into binding buffer. After baseline measurement in the binding buffer alone, the binding kinetics were monitored by dipping the biosensors in wells containing the target protein at the indicated concentration (association step) for 3,600 s and then dipping the sensors back into baseline/buffer (dissociation) for 7,200 s.

Plaque assay

Vero-furin or Vero-hACE2-TMPRSS2 cells were seeded at a density of 2.5×10^5 cells per well in flat-bottom 12-well tissue culture plates. The following day, medium was removed and replaced with 200 μL of 10-fold serial dilutions of the material to be titrated, diluted in DMEM+2% FBS, and plates incubated at 37°C with rocking at regular intervals. One h later, 1 mL of methylcellulose overlay was added. Plates were incubated at 37°C for 72 h, then fixed with 4% paraformaldehyde (final concentration) in PBS for 20 min. Fixed cell monolayers were stained with 0.05% (w/v) crystal violet in 20% methanol and washed twice with distilled, deionized water.

Measurement of viral burden

Tissues were weighed and homogenized with zirconia beads in a MagNA Lyser instrument (Roche Life Science) in 1,000 μL of DMEM media supplemented with 2% heat-inactivated FBS. Tissue homogenates were clarified by centrifugation at 10,000 rpm for 5 min and stored at −80°C. RNA was extracted using the MagMax mirVana Total RNA isolation kit (Thermo Scientific) on a Kingfisher Flex extraction robot (Thermo Scientific). RNA was reverse transcribed and amplified using the TaqMan RNA-to-CT 1-Step Kit (ThermoFisher). Reverse transcription was carried out at 48°C for 15 min followed by 2 min at 95°C. Amplification was accomplished over 50 cycles as follows: 95°C for 15 s and 60°C for 1 min. Copies of SARS-CoV-2 N gene RNA in samples were determined using a previously published assay (Case et al., 2020; Hassan et al., 2020). Briefly, a TaqMan assay was designed to target a highly conserved region of the N gene (Forward primer: ATGCTGCAATCGTGCTACAA; Reverse primer: GACTGCCGCCTCTGCTC; Probe: /56-FAM/TCAAGGAAC/ZEN/AACATTGCCAA/3IABkFQ/). This region was included in an RNA standard to allow for copy number determination down to 10 copies per reaction. The reaction mixture contained final concentrations of primers and probe of 500 and 100 nM, respectively.

Cytokine and chemokine mRNA measurements

RNA was isolated from lung homogenates as described above. cDNA was synthesized from DNase-treated RNA using the High-Capacity cDNA Reverse Transcription kit (Thermo Scientific) with the addition of RNase inhibitor following the manufacturer's protocol. Cytokine and chemokine expression was determined using TaqMan Fast Universal PCR master mix (Thermo Scientific) with commercial primers/probe sets specific for *IFN-g* (IDT: Mm.PT.58.41769240), *IL-6* (Mm.PT.58.10005566), *IL-1b* (Mm.PT.58.41616450), *Tnfa* (Mm.PT.58.12575861), *CXCL10* (Mm.PT.58.43575827), *CCL2* (Mm.PT.58.42151692), *CCL5* (Mm.PT.58.43548565), *CXCL11*

Please cite this article in press as: Case et al., Ultrapotent miniproteins targeting the SARS-CoV-2 receptor-binding domain protect against infection and disease, Cell Host & Microbe (2021), https://doi.org/10.1016/j.chom.2021.06.008

(Mm.PT.58.10773148.g), *Ifnb* (Mm.PT.58.30132453.g), *CXCL1* (Mm.PT.58.42076891) and results were normalized to *GAPDH* (Mm.PT.39a.1) levels. Fold change was determined using the $2^{-\Delta\Delta Ct}$ method comparing treated mice to naive controls.

Lung pathology

Animals were euthanized before harvest and fixation of tissues. The left lung was first tied off at the left main bronchus and collected for viral RNA analysis. The right lung was inflated with approximately 1.2 mL of 10% neutral buffered formalin using a 3-mL syringe and catheter inserted into the trachea. Tissues were embedded in paraffin, and sections were stained with hematoxylin and eosin. Slides were scanned using a Hamamatsu NanoZoomer slide scanning system, and images were viewed using NDP view software (ver.1.2.46).

Respiratory mechanics

Mice were anesthetized with ketamine/xylazine (100 mg/kg and 10 mg/kg, i.p., respectively). The trachea was isolated via dissection of the neck area and cannulated using an 18-gauge blunt metal cannula (typical resistance of 0.18 $cmH_2O.s/mL$), which was secured in place with a nylon suture. The mouse then was connected to the flexiVent computer-controlled piston ventilator (SCIREQ Inc.) via the cannula, which was attached to the FX adaptor Y-tubing. Mechanical ventilation was initiated, and mice were given an additional 100 mg/kg of ketamine and 0.1 mg/mouse of the paralytic pancuronium bromide via intraperitoneal route to prevent breathing against the ventilator and during measurements. Mice were ventilated using default settings for mice, which consisted in a positive end expiratory pressure at 3 cm H_2O, a 10 mL/kg tidal volume (Vt), a respiratory rate at 150 breaths per minute (bpm), and a fraction of inspired oxygen (FiO_2) of 0.21 (*i.e.*, room air). Respiratory mechanics were assessed using the forced oscillation technique, as previously described (McGovern et al., 2013), using the latest version of the flexiVent operating software (flexiWare v8.1.3). Pressure-volume loops and measurements of inspiratory capacity also were performed.

Neutralization assay

Serial dilutions of binder proteins or serum and tissue homogenates were incubated with 10^2 focus-forming units (FFU) of SARS-CoV-2 for 1 h at 37°C. Binder-virus complexes were added to Vero E6 (WA1/2020) or Vero-hACE2-TMPRSS2 (B.1.1.7, WA1/2020 E484K/N501Y/D614G, and serum and tissue homogenates) cell monolayers in 96-well plates and incubated at 37°C for 1 h. Subsequently, cells were overlaid with 1% (w/v) methylcellulose in MEM supplemented with 2% FBS. Plates were harvested 24-30 h later by removing overlays and fixed with 4% PFA in PBS for 20 min at room temperature. Plates were washed and sequentially incubated with an oligoclonal pool of SARS2-2, SARS2-11, SARS2-16, SARS2-31, SARS2-38, SARS2-57, and SARS2-71 anti-spike protein antibodies (VanBlargan et al., 2021) and HRP-conjugated goat anti-mouse IgG in PBS supplemented with 0.1% saponin and 0.1% bovine serum albumin. SARS-CoV-2-infected cell foci were visualized using TrueBlue peroxidase substrate (KPL) and quantitated on an ImmunoSpot microanalyzer (Cellular Technologies). Data were processed using Prism software (GraphPad Prism 8.0).

ELISA

To assess binder immunogenicity, C-terminal biotinylated LCB1v1.3 was immobilized on streptavidin-coated plates (RayBiotech #7C-SCP-1) at 2.5 μg/mL in 100 μL total volume per well and incubated at 4°C overnight. Plates were washed with wash buffer (TBS + 0.1% (w/v) BSA + 0.05% (v/v) Tween20) and blocked with 200 μL/well blocking buffer (TBS + 2% (w/v) BSA + 0.05% (v/v) Tween20) for 1 h at room temperature. Plates were rinsed with wash buffer using 200 μL/well, and 100 μL of 1:100 diluted sera samples in blocking buffer were added to respective wells. For a positive control, Fc-RBD was serially diluted 1:5 starting at 240 ng/mL in 100 μL of blocking buffer. All samples were incubated for 1 h at room temperature. Plates were washed using 200 μL/well of wash buffer. For the serum samples, HRP-conjugated horse anti-mouse IgG antibody (Vector Laboratories #PI-2000-1) was diluted 1:200 in blocking buffer, and 100 μL was incubated in each well at room temperature for 30 min. For the positive control, HRP-conjugated mouse anti-human IgG antibody (Invitrogen #05-4220) was diluted 1:500 in blocking buffer, and 100 μL was incubated in each well at room temperature for 30 min. Plates were rinsed with wash buffer, and 100 μL of TMB (SeraCare) was added to each well for 2 min. The reaction was quenched by adding 100 μL of 1N HCl. Optical densities were determined at 450nm on a Synergy Neo2 plate reader (BioTek Instruments).

To determine LCB1v1.3 binder concentrations in tissues, a competitive ELISA was performed. Maxisorp 96-well plates (Thermo Scientific #44-2404-21) were coated with 4 ng/μL Hexapro in 1X TBS-T (20X TBS-T: Thermo Scientific #28360) for 1 h at 37°C. Plates were washed four times with 300 μL of 1X TBS-T before blocking with 200 μL SuperBlock blocking buffer (Thermo Scientific #37515) for 1 h at 37°C. Plates were washed four times with 300 μL of 1X TBS-T. 100 μL 2 nM hACE2-Fc in 1X TBS-T was added to all wells. 16.7 μL of 300 nM LCB1v1.3 was added to the first row of columns 1-3 as a standard, and 16.7 μL of tissue sample was added to the first row of other columns. All samples were processed in triplicate. Samples and standards were serially diluted in a 1:3 fashion and then incubated for 1 h at 37°C. Plates were washed four times with 300 μL of 1X TBS-T. 50 μL of 1:5000 anti-hFc-HRP secondary antibody (Invitrogen #A18817) was added to each well and incubated for 1 h at 37°C. Plates were washed four times with 300 μL of 1X TBS-T. 100 μL TMB (Thermo Scientific #34028) was added to each well, and plates were placed on an orbital shaker for 30 s before addition of 100 μL of 1 N HCl to stop the reaction. Plates were read for absorbance at 450 nm on a SpectraMax Plus 384 plate reader. Data were analyzed by nonlinear regression in GraphPad Prism to obtain IC_{50} values. Sample LCB1v1.3 concentrations were determined by using the ratio of standard IC_{50}/standard concentration to sample IC_{50}/sample concentration.

Please cite this article in press as: Case et al., Ultrapotent miniproteins targeting the SARS-CoV-2 receptor-binding domain protect against infection and disease, Cell Host & Microbe (2021), https://doi.org/10.1016/j.chom.2021.06.008

To determine LCB1-Fc concentrations in tissues, a direct ELISA was performed. Maxisorp 96-well plates (Thermo Scientific #44-2404-21) were coated with 4 ng/μL of Hexapro in 1X TBS-T (20X TBS-T: Thermo Scientific #28360) for 1 h at 37°C. Plates were washed four times with 300 μL of 1X TBS-T before blocking with 200 μL SuperBlock blocking buffer (Thermo Scientific #37515) for 1 h at 37°C. Plates were washed four times with 300 μL of 1X TBS-T. 100 μL 1X TBS-T was added to all wells. 16.7 μL of 300 nM LCB1-Fc was added to the first row of columns 1-3 as a standard, and 16.7 μL of tissue sample was added to the first row of other columns. All samples were processed in duplicate. Samples and standards were serially diluted in a 1:3 fashion and then incubated for 1 h at 37°C. Plates were washed four times with 300 μL of 1X TBS-T. 50 μL of 1:5000 anti-hFc-HRP secondary antibody (Invitrogen #A18817) was added to each well and incubated for 1 h at 37°C. Plates were washed four times with 300 μL of 1X TBS-T. 100 μL TMB (Thermo Scientific #34028) was added to each well, and plates were placed on an orbital shaker for 30 s before adding 100 μL of 1 N HCl to stop the reaction. Plates were then read for absorbance at 450 nm on a SpectraMax Plus 384 plate reader. Data were analyzed by nonlinear regression in GraphPad Prism. Sample LCB1-Fc concentrations were determined using a linear equation between two adjacent points in the standard curve and multiplying by the appropriate dilution factor.

QUANTIFICATION AND STATISTICAL ANALYSIS

Statistical significance was assigned when *P value*s were < 0.05 using Prism Version 8 (GraphPad). Tests, number of animals, median values, and statistical comparison groups are indicated in each of the Figure legends. Analysis of weight change was determined by two-way ANOVA. Changes in functional parameters or immune parameters were compared to control binder-treated animals and analyzed by one-way ANOVA with multiple comparisons tests. Statistical analyses of viral burden between two groups were determined by Mann-Whitney test.